

Рис.5 Снижение выбросов вредных веществ с отработавшими газами за счет использования альтернативных топлив

Поэтому хотим мы или не хотим, но решение этой проблемы по существу подводит нас к необходимости создания многотопливных модификаций бензиновых и дизельных двигателей внутреннего сгорания, а в перспективе к единой многотопливной модификации ДВС в составе КЭУ и в модульных схемах силовых установок с регулируемой степенью сжатия и рабочим объемом для конкурентоспособных автотранспортных средств с наилучшими эколого-экономическими характеристиками.

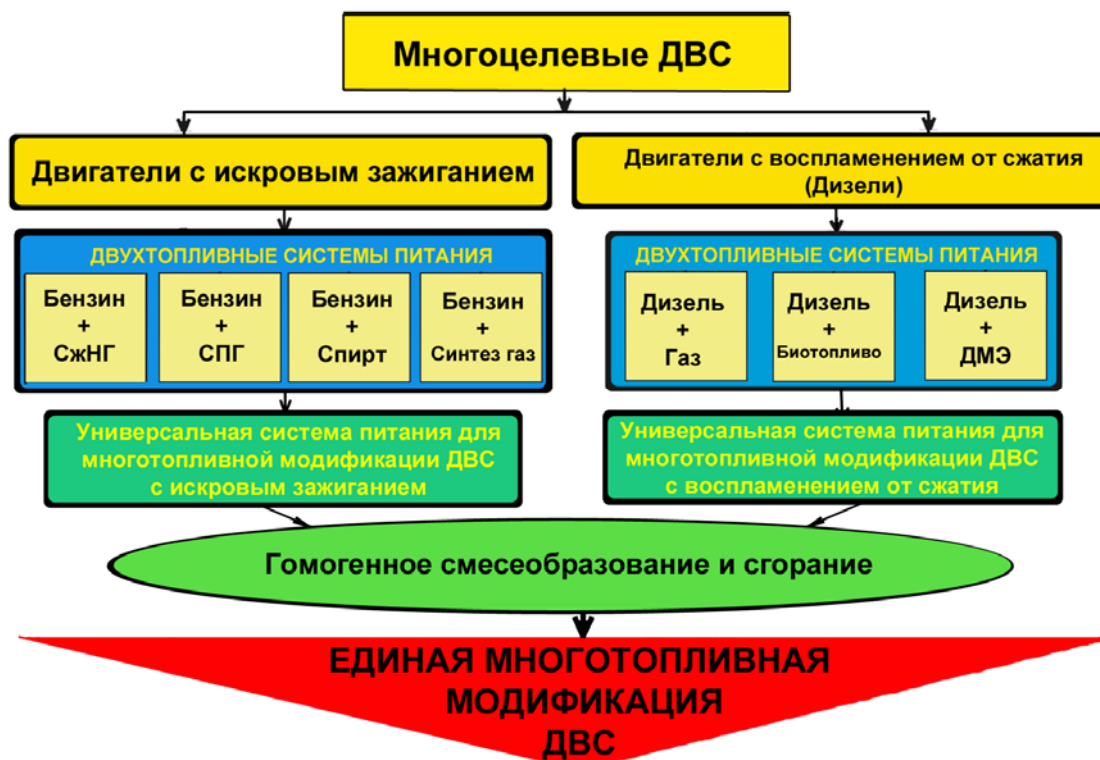


Рис.6

#### Литература:

1. Кутенёв В.Ф., Токарев А.А. Работы по улучшению топливной экономичности АТС / Автомобильная промышленность, 1988 г., №2, с. 3-4.
2. Ипатов А.А., Эйдинов А.А. / Электромобили и автомобили с комбинированными энергоустановками (КЭУ) / НАМИ - М., - 2004, с.328
3. Зленко М.А., Кутенев В.Ф. Двигатели с регулируемым рабочим объемом и степенью сжатия.: Учебное пособие / МАМИ – М., - 2006, с.118
4. Гиринович М.П. Исследование процессов образования оксидов азота при сгорании топлив в перспективных дизелях. / Автореферат диссертации на соискание ученой степени канд. техн. наук. – М., - 2006.

### MODELING OF SOOT FORMATION IN INTERNAL COMBUSTION ENGINES

**Frolov S.M., Basevich V.Ya., Vlasov P.A., Skripnik A.A.**

(Semenov Institute of Chemical Physics, 4, Kosigin Str., Moscow 119991 Russia)

**Priesching P., Tatschl R.**

(AVL LIST GMBH, 1, Hans-List-Platz, Graz A-8020, Austria )

**Introduction.** Soot formation is a complex process, which incorporates many chemical and physical steps: (1) homogeneous inception of large molecular precursors, (2) surface growth in the reactions with the gas-phase active species, (3) coalescent coagulation to form larger particles, and, finally, (4) agglomeration of the primary particles to form chain-like aggregates.

The formation of molecular precursors is the first important step in the course of soot formation. Regardless the initial fuel involved, the hydrocarbon fuel undergoes either pure or oxidative pyrolysis, degrading into small hydrocarbon radicals. Under fuel-rich conditions, the small radicals react, leading to the formation of smaller hydrocarbons, particularly acetylene ( $C_2H_2$ ). Then, large hydrocarbon molecules containing a sufficiently large number of carbon atoms such as polyynes ( $C_{2n}H_2$ ,  $n = 2, 3, \dots$ ) and polycyclic aromatic hydrocarbons (PAHs) are built up, that are commonly regarded as the molecular soot precursors.

Depending on the type of molecular precursors assumed to be present, several competing theories, such as the PAH model or the polyynes model, have been proposed. In the H-abstraction-acetylene-addition (HACA) mechanism, aromatic species like benzene, toluene, naphthalene, etc. are considered as islands of stability in an infinite sea of possible molecular structures which might be formed through molecular growth. The polyynes model assumes that every radical capable of forming polyynes complexes becomes a center of polymerization. A polyynes molecule and a polyynes radical or two polyynes molecules react to form the polyynes complexes. Under high temperature conditions, when C-H bonds are relatively loose, the carbon skeletons of acetylene and polyynes molecules persist in the gas-phase as the most stable structures of small carbon clusters due to their high thermodynamic stability. Recent experiments and theoretical studies have discovered that the most stable structures of carbon clusters up to  $C_{20}$  are chains and monocycles. This finding supports the polyynes mechanism recently developed on the basis of the fast chemical aggregation theory in the works.

For modeling soot formation in internal combustion engines using CFD software there is a need in simple and efficient soot models predicting satisfactorily the soot yield under different operation conditions. The detailed kinetic models of soot formation incorporating all the processes mentioned above can be used for validating such models.

The objective of this study was to develop a computationally efficient overall soot model based on the detailed soot formation model.

**1 Detailed mechanism.** Semenov Institute of Chemical Physics has been involved in soot formation modeling for a long time. Recently, the most detailed mechanism of soot formation has been developed by joint efforts of Semenov Institute and Universität Heidelberg. For example, Vlasov reported the kinetic scheme of soot formation process during pyrolysis of various aliphatic and aromatic hydrocarbons. It combines the mechanisms of formation of polyaromatic hydrocarbons, polyynes, two mechanisms of soot precursor formation due to condensation of polyaromatic and polyynes molecules, soot particle growth by the reactions of HACA mechanism and polyynes molecule addition, the mechanism of acetylene pyrolysis and pure carbon cluster formation. Later, the mechanism of *n*-heptane oxidation was added into this detailed kinetic scheme of soot formation process. As a result, the complete detailed kinetic scheme of soot formation process incorporates 1850 gas-phase reactions between 186 species and 100 heterogene-

ous reactions with participation of four ensembles of microheterogeneous particles of different types. The rate coefficients of some important reactions have pressure dependence. Thus, the gas phase reaction mechanism consists of a complete kinetic scheme of polyaromatic hydrocarbon formation for laminar premixed acetylene and ethylene flames with all corrections, the kinetic scheme of acetylene pyrolysis, the kinetic scheme of polyynene molecule formation, the kinetic scheme of pure carbon cluster formation up to C<sub>30</sub>, and the kinetic scheme of *n*-heptane oxidation.

The gas-phase kinetic scheme of polyaromatic hydrocarbon formation describes the pyrolysis and oxidation of C<sub>1</sub> and C<sub>2</sub> species, the formation of higher linear hydrocarbons up to C<sub>6</sub> species, the formation of benzene and further reactions leading to pyrene and the oxidation pathways of the aromatic species. The gas-phase reaction mechanism of the model considered consists of the reactions of the following species: H<sub>2</sub>/O<sub>2</sub>, HO<sub>2</sub>/H<sub>2</sub>O<sub>2</sub>, CO/CO<sub>2</sub>, C/C<sub>2</sub>/ . . . /C<sub>30</sub>, CH, HCO, CH<sub>2</sub>, CH<sub>2</sub><sup>\*</sup>, CH<sub>2</sub>O, CH<sub>3</sub>, CH<sub>3</sub>O/CH<sub>2</sub>OH, CH<sub>4</sub>, CH<sub>3</sub>OH, C<sub>2</sub>H, HCCO, C<sub>2</sub>H<sub>2</sub>, CH<sub>2</sub>CO/HCCOH, C<sub>2</sub>H<sub>3</sub>, C<sub>2</sub>H<sub>4</sub>, C<sub>2</sub>H<sub>5</sub>, C<sub>2</sub>H<sub>6</sub>, C<sub>2</sub>O, C<sub>2</sub>H<sub>3</sub>O, C<sub>3</sub>H<sub>2</sub>/C<sub>3</sub>H<sub>3</sub>/C<sub>3</sub>H<sub>4</sub>, C<sub>4</sub>H/C<sub>4</sub>H<sub>2</sub>, C<sub>4</sub>H<sub>3</sub>/C<sub>4</sub>H<sub>4</sub>, C<sub>4</sub>H<sub>5</sub>/C<sub>4</sub>H<sub>6</sub>, C<sub>5</sub>H<sub>2</sub>/C<sub>5</sub>H<sub>3</sub>, C<sub>6</sub>H/C<sub>6</sub>H<sub>2</sub>, C<sub>6</sub>H<sub>3</sub>/C<sub>6</sub>H<sub>4</sub>, C<sub>6</sub>H<sub>5</sub>/C<sub>6</sub>H<sub>6</sub>, C<sub>6</sub>H<sub>7</sub>/C<sub>6</sub>H<sub>8</sub>, benzene/phenyl, polyynes (C<sub>8</sub>H<sub>2</sub>/C<sub>8</sub>H, C<sub>10</sub>H<sub>2</sub>/C<sub>10</sub>H, C<sub>12</sub>H<sub>2</sub>/C<sub>12</sub>H, C<sub>14</sub>H<sub>2</sub>), phenylacetylene, phenylvinyl/styrene, naphthalene, ethynyl naphthalene, phenanthrene, pyrene, biphenyl, benzene oxidation, PAH oxidation by OH, and PAH oxidation by O.

A key aspect of the soot formation process is the deposition of soot mass through reactions of gaseous species with the soot particle surface. In the model available, a minimal mechanism of surface growth of soot particles is considered. Soot precursors are formed in condensation reactions of pyrene, phenanthrene, and biphenyl molecules (the HACA pathway) and the polyynene molecules C<sub>8</sub>H<sub>2</sub>, C<sub>10</sub>H<sub>2</sub>, and C<sub>12</sub>H<sub>2</sub> (the polyynene pathway). The reactions of the soot particles with active sites formed through the HACA pathway with polyynene molecules and polyynene radicals, which create new active sites on their surface, lead to the formation of active soot particles similar to those formed through the polyynene pathway. After this transformation, only active soot particles are considered in the model. These soot particles react with the most reactive gas-phase species (C<sub>2</sub>H<sub>2</sub>, C<sub>2</sub>H, C<sub>2</sub>, C<sub>4</sub>H<sub>4</sub>, C<sub>4</sub>H<sub>2</sub>, C<sub>4</sub>H, C<sub>4</sub>, C<sub>6</sub>H<sub>2</sub>, C<sub>6</sub>H, C<sub>6</sub>, C<sub>8</sub>H<sub>2</sub>, C<sub>8</sub>H, C<sub>8</sub>, C<sub>10</sub>H<sub>2</sub>, C<sub>10</sub>H, C<sub>10</sub>, C<sub>12</sub>H<sub>2</sub>, C<sub>12</sub>H, and C<sub>12</sub>) and participate in condensation reactions with pyrene, phenanthrene, and naphthalene and in coagulation reactions. The soot formation mechanism is included into the MACRON code, which is used for mechanism validation and all calculations presented in this report.

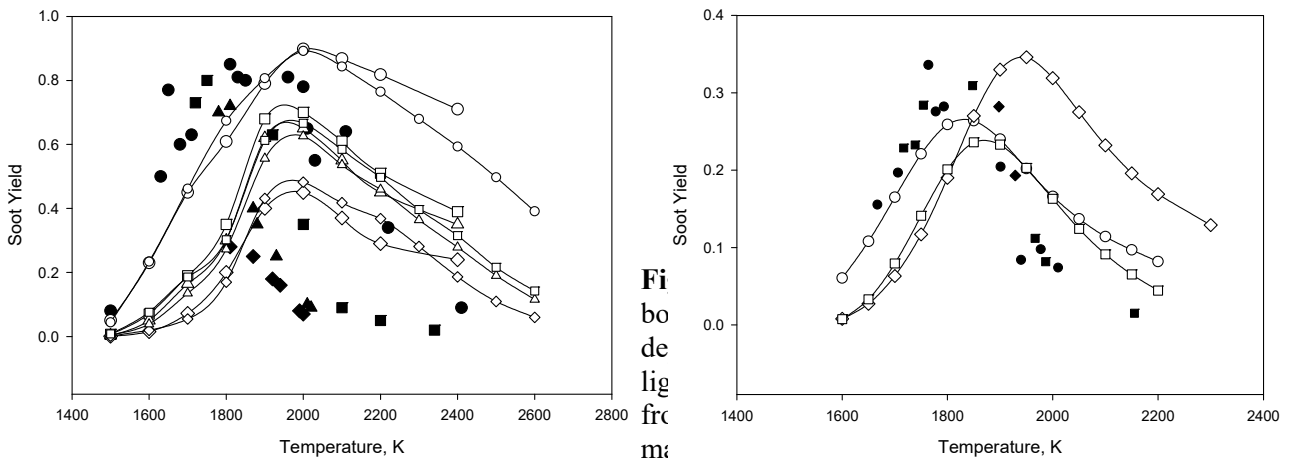
For validating the detailed mechanism of soot formation, we compared the results of calculations of the temperature dependencies of the soot yield, the observable rate of soot particle growth and the induction time of soot formation process during pyrolysis of various hydrocarbons for different concentrations of carbon atoms in the reaction mixture with the experimental results from the cw-laser extinction measurements behind reflected shock waves (Fig. 1). The experimentally measured and calculated values of the soot yield and the induction time of soot formation are in good agreement. This is indicative of a qualitative and quantitative relevance of the kinetic scheme considered.

Next, we compared the experimentally and calculated characteristics of soot formation process during rich oxidation of the mixtures of *n*-heptane, methane, and propane with oxygen under conditions realized behind reflected shock waves at elevated pressures (see Fig. 2). A combination of the extinction-scattering technique at  $\lambda = 488$  and 632.8 nm was used for time resolved measurements of soot particle diameter and number

density and the traditional extinction technique was applied to determine the soot yield and induction times.

The difference in the soot yield during rich oxidation of various hydrocarbons is not significant. One can suppose that the major portion of a fuel is pyrolyzed with the formation of intermediate species. As they are formed, a competition occurs between molecular growth and oxidative reactions. Whereas the major portion of pyrolysis intermediates is eventually oxidized, a large portion of the carbon-containing species participates in the molecular growth process.

Oxidative reactions lead to a variety of oxygen-containing intermediates and products including CO, CO<sub>2</sub>, and H<sub>2</sub>O. As a result, the soot yield decreases as compared with the situation of a pure pyrolysis.



Open symbols designate the results of detailed calculations and closed symbols stand for the experimental results. The number density and the traditional extinction technique was applied to determine the soot yield and induction times

of (circles) *n*-heptane ( $[C] = 5.9 \text{ mol/m}^3$ ,  $\phi = 5$ ), (squares) methane ( $[C] = 7.6 \text{ mol/m}^3$ ,  $\phi = 5$ ), and (diamonds) propane ( $[C] = 6.0 \text{ mol/m}^3$ ,  $\phi = 5$ ), behind shock wave at pressure of 40 bar

The temperature dependences of the mean diameter of soot particles formed during rich oxidation of *n*-heptane obtained from the light scattering measurements ( $\lambda = 488 \text{ nm}$ ) and calculated with the use of the detailed kinetic model of soot formation were compared for various pressures behind reflected shock wave and a satisfactory agreement was noticed.

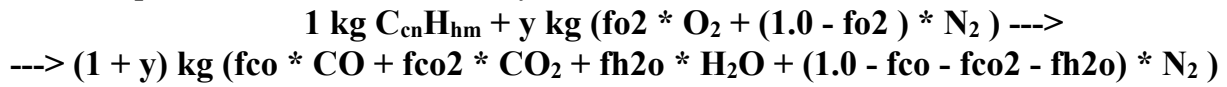
The influence of the concentration of carbon atoms in the reacting mixture and the pressure influence behind reflected shock wave on the soot yield during rich oxidation of *n*-heptane were also studied. If the concentration of carbon atoms in the reacting mixture is preserved constant for various pressures, the pressure influence on the soot yield is insignificant and the variation of the concentration of carbon atoms in the reacting mixture, which occurs if the pressure is changed, provides the major contribution into the variation of the soot yield value.

**2 Overall Mechanism.** The model described in Section 2 cannot currently be implemented into the CFD code due to the excessively large number of reactive species involved and hence unaffordable CPU time. To overcome this problem we have devel-

oped an approach based on the implications obtained from the analysis of the detailed mechanism. These implications are listed below:

- (1) In order to avoid soot yields exceeding 1.0 it is necessary to take into account fuel depletion in the soot formation reaction.
- (2) In order to correctly simulate soot oxidation in fuel-rich mixtures, it is necessary to take into account soot oxidation by both oxygen and water.
- (3) The reaction steps dealing with hydrogen and carbon monoxide formation and oxidation in the course of fuel oxidation can be assumed infinitely fast. Therefore fuel can be assumed to oxidize to CO<sub>2</sub> and H<sub>2</sub>O rather than to CO and H<sub>2</sub>O.
- (4) It can be roughly assumed that oxygen and water are not consumed in the soot oxidation reactions as it is done in the majority of available overall soot oxidation mechanisms.

In view of the implications (1) to (4), the new overall mechanism of soot formation can be represented as follows. The Symbolic reaction of fuel oxidation is:



where  $hm=2(cn)+2$  for saturated hydrocarbons, and  $fo_2, fco, fco_2, fh_2o$  are the stoichiometric coefficients of O<sub>2</sub>, CO, CO<sub>2</sub> and water, respectively. In terms of particular species, the symbolic reactions of soot formation and oxidation in Table 2 are:



where ‘‘Soot’’ is represented by the C atom. Since water participates in the soot oxidation reaction, the ‘‘Product’’ is worth to be attributed to either CO<sub>2</sub> or N<sub>2</sub> in order to keep minimal the number of reactive species. Each reaction is characterized by the reaction rate  $W_i$  ( $i=I, II, III$ )

$$W_i = A_i \exp\left(-\frac{E_i}{RT}\right) \prod [X_j]$$

where  $T$  is the temperature,  $E_i$  is the activation energy, and  $\prod [X_j]$  are the products of volume fractions of species participating in the reaction. The rates of reactions (I), (II), and (III) are written in the form:

**Table 1:** Kinetic parameters ( $A$  and  $E$ ) of reactions (I), (II) and (III) depending on the mixture equivalence ratio (at pressure ranging from 50 to 200 bar and temperature ranging from 1400 to 3000 K).

Fuel	Reaction	$\Phi$	1.5	1.54	3	4	5	6	8
C <sub>7</sub> H <sub>16</sub>	I	A		5.0E+10	5.0E+10		5.0E+10		
		E		6.0E+04	6.0E+04		6.0E+04		
	II	A		5.2E+12	5.2E+12		5.2E+12		
		E		0.0E+00	0.0E+00		0.0E+00		
	III	A		8.0E+10	8.0E+09		8.0E+09		
		E		4.0E+04	7.0E+04		9.0E+04		
CH <sub>4</sub>	I	A				1.0E+10		1.0E+10	1.0E+10
		E				6.0E+04		7.0E+04	7.0E+04
	II	A				5.2E+12		5.2E+12	5.2E+12
		E				0.0E+00		0.0E+00	0.0E+00
	III	A				1.0E+16		1.0E+10	1.0E+10
		E				1.0E+05		6.5E+04	6.5E+04
C <sub>3</sub> H <sub>8</sub>	I	A	8.0E+10		8.0E+10		8.0E+10		
		E	6.0E+04		6.0E+04		6.0E+04		
	II	A	5.2E+12		5.2E+12		5.2E+12		

		<b>E</b>	0.0E+00		0.0E+00		0.0E+00	
	<b>III</b>	<b>A</b>	1.0E+15		6.0E+09		6.0E+09	
		<b>E</b>	1.0E+05		7.0E+04		8.5E+04	

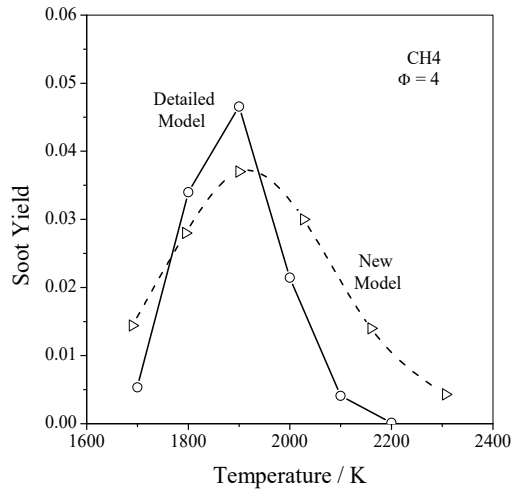


**Fig. 3:** Soot yield vs. temperature at methane oxidation in air at  $p = 50$  atm, and  $\Phi = 4$  predicted by the new model (triangles) and detailed (circles) model

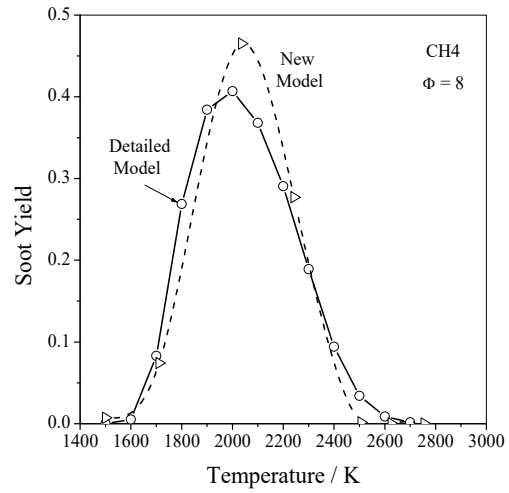


**Fig. 4:** Soot yield vs. temperature at methane oxidation in air at  $p = 50$  atm, and  $\Phi = 8$  predicted by the new model (triangles) and detailed (circles) model

$$W_I = 2(cn)K_I[X_{C_{cn}H_{hm}}][X_{C_{cn}H_{hm}}];$$

$$W_{II} = 2K_{II}[X_C][X_C][X_{O_2}]; \quad W_{III} = K_{III}[X_C][X_{H_2O}],$$

where  $K_i = A_i \exp(-E_i/RT)$ . Table 1 shows the optimized values of kinetic parameters  $A$  and  $E$  for reactions (I), (II), and (III). These parameters were obtained for different values of the equivalence ratio  $\Phi$  (from 1.5 to 8) and for different fuels (methane, propane, and n-heptane). These values are valid for pressures from 50 to 200 bar and temperatures from 1400 to 3600 K. Figures 3 to 6 show the comparison of soot yields predicted by the detailed solution (solid curves) and the new model (dashed curves) at isothermal soot formation with the residence time of 3 ms. It is seen that the new model predicts the bell-shaped curves for the soot yield vs. temperature and provides satisfactory agreement with the detailed model in the most cases considered.

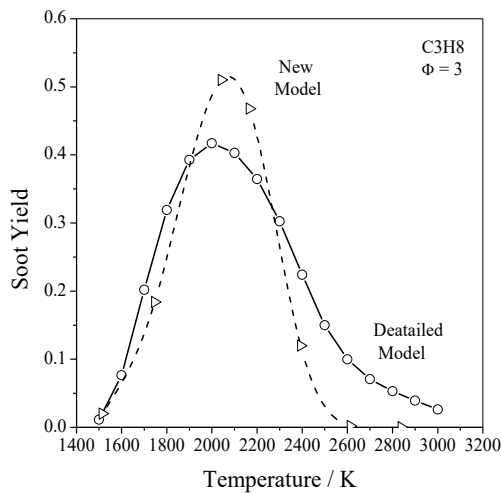


**Fig. 5:** Soot yield vs. temperature at propane oxidation in air at  $p = 50$  atm, and  $\Phi = 3$  predicted

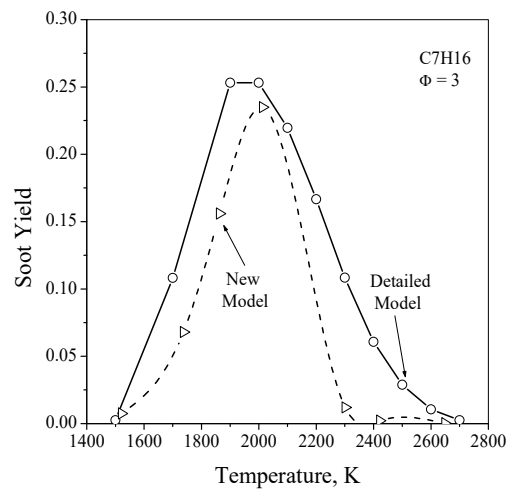


**Fig. 6:** Soot yield vs. temperature at n-heptane oxidation in air at  $p = 50$  atm and  $\Phi = 3$  predicted

by the new model (triangles) and detailed (circles) model

### 3. Validation of overall model

#### 3.1 Engine and operating conditions.

The engine used for the validation study is a single-cylinder research engine with electro hydraulic valve actuation and three intake ports with swirl flaps. An  $\omega$ -shaped piston bowl has been chosen for this study. The main engine and injection system data are summarized in Table 2.

Validation of the overall model is presented for one operating point with conventional Diesel combustion. For this operating point DoE plans have been used for the design of the calculation campaign. This means that for this point a significant number of combustion system variations have been applied by simultaneously changing the start of injection (SOI), residual gas amount (EGR), swirl level and injection pressure. The following table shows the main specifications and the range of parameter variations for the case studied.

For the entire set of DoE based operating parameter variations test-bed measurements have been carried out for the investigated speed/load points. The measured in-cylinder pressure traces and engine out emission data for NO, soot, CO and unburned hydrocarbons were then used for the assessment of the performance of the combustion/emissions model suite adopted in the CFD calculations.

**3.2 Computational details.** In order to enable the large number of 3D CFD calculations of the DoE matrix to be performed within reasonable time, the calculations were done on an engine segment mesh covering 1/8 of the cylinder/piston bowl arrangement around one single fuel spray assuming cyclic symmetry using AVL FIRE code. Fig. 7a shows a snapshot of the mesh topology at 40 degree crank-angle BTDC position adopting a spray aligned mesh block in order to exclude undesired numerical influences on the spray/combustion results. The mesh size varies over the cycle between 68.000 (BDC) and 24.000 (TDC).

The engine segment calculations for each DoE matrix point were started at the time of inlet valve closure (115 degree crank-angle BTDC) and commenced until opening of the exhaust valves (138 degree crank-angle ATDC).

The crank angle increment during compression phase has been chosen with 1 deg CA. During the injection and combustion phase the increment has been reduced to 0.1 deg CA in order to accurately resolve the fast chemical and physical processes.

The gas side initial conditions at the time of inlet valve closure, i.e. in-cylinder pressure, temperature and residual gas mass fraction, as well as the wall temperature boundary conditions were taken from 1D cycle simulations adopting the AVL BOOST code.

A solid body rotation of the in-cylinder flow field at the time of inlet-valve closure was prescribed, with the swirl levels and turbulence intensities extracted from preceding calculations of the entire intake stroke adopting a full 3D computational model.

ed by the new model (triangles) and detailed (circles) model

Bore	85 mm
Stroke	94 mm
Displacement	533.4 cm <sup>3</sup>
Compression ratio	16:1
Injection system BOSCH	Piezo CR
Number of injection holes	8
Spray angle	158 deg

	Load Point
Engine speed	3000 rpm
IMEP	8.3 bar
SOI	1 – 10 deg BTDC
EGR	12 – 20 %
Swirl	0 – 74 %
Inj. Pressure	1200 – 1600 bar

The fuel side boundary conditions, i.e. hydraulic injection timing and injection rates for the different injection pressure levels were obtained on the basis of 1D hydraulic simulations adopting the AVL HYDSIM code. Parameterization of the hydraulic model was conducted on the basis of selected 3D nozzle flow simulations. Figure 8 shows the comparison of predicted and measured soot emission indices for different operating conditions within the load point defined in Table 3. Excellent agreement between calculations and experimental measurements is worth mentioning.

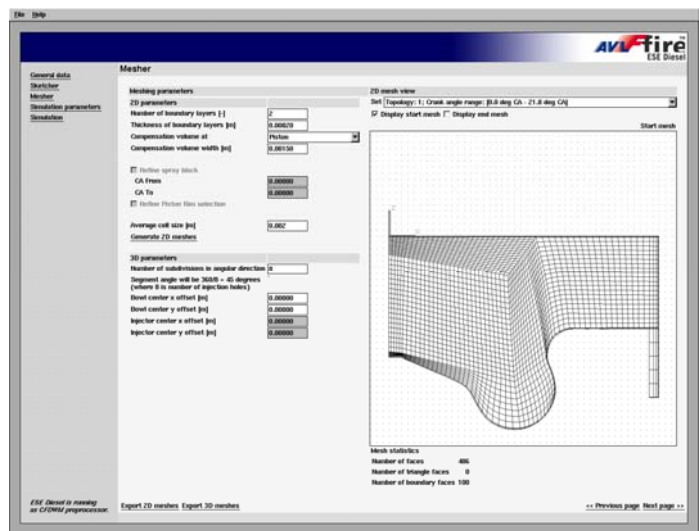


**Fig. 7:** Set-up of the engine segment model and the CFD calculation within the FIRE Engine Simulation Environment Diesel (ESE Diesel)

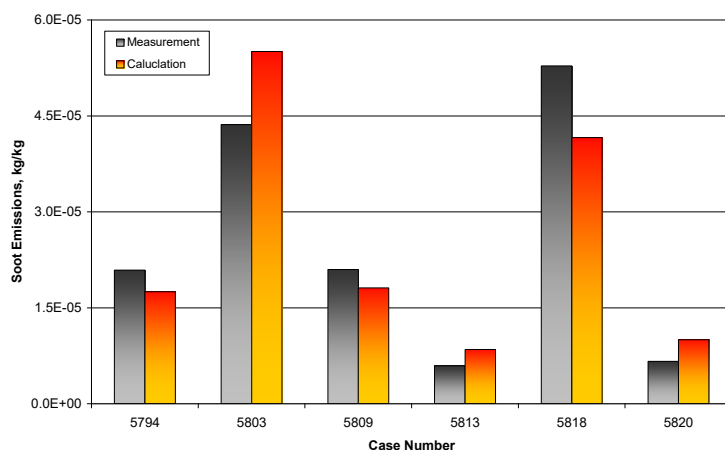


**Fig. 8:** Comparison of predicted and measured soot emission indices for conditions in Table 3

### Concluding remarks.

This paper briefly describes the most detailed soot formation mechanism currently available, which includes all known alternative roots of soot formation

during pyrolysis and oxidation of hydrocarbons. It accumulates the results of detailed calculation of soot yield during pyrolysis and oxidation of *n*-heptane–air, methane–air, and propane–air mixtures within the temperature range from 1500 to 3000 K, pressure range from 50 to 200 bar, and the range of the equivalence ratio from 0 to 8.

The detailed calculations were made using the MACRON code for the homogeneous conditions realized in shock-tube experiments on soot formation behind reflected shock waves with the reaction time of 3 ms. The new overall soot formation model has been developed. The overall model reflects well all qualitative features of the detailed soot formation model. Quantitatively, the overall model corresponds with the predictions of the detailed model within a factor of 2-3. For model validation studies, a single-cylinder research engine with electro hydraulic valve actuation and three intake ports with swirl flaps was used. 3D calculations using AVL FIRE code and the new overall soot formation model have been performed and compared with the measurements. Excellent agreement of predicted and measured results was obtained.

**Acknowledgements.** This study was partly supported by AVL LIST GmbH and Russian Foundation for Basic Research grant #05-08-18200.

## **BOSCH CNG STRATEGY AND TECHNOLOGY**

### **NATURAL-GAS MOTRONIC FOR SUSTAINABLE MOBILITY**

**Robert Bosch GmbH, Stuttgart, Germany**

Natural gas is a fossil fuel with a future. It is produced without the need for extensive refining, and its combustion places far less load on the environment than gasoline or diesel. For the special requirements of natural-gas engines Bosch has developed special technologies for gas injection and engine management.

#### **A fuel with many advantages**

There is great potential for Compressed Natural Gas (CNG) due to it having very low emissions. Compared to gasoline, CNG combustion produces about 25% less carbon dioxide (CO<sub>2</sub>). Furthermore, CNG has a great potential for reducing untreated emissions. The exhaust gas is odorless and contains no particles.

CNG also has an advantage when being prepared as a fuel: it needs no additives and its production does without complicated refining processes. Another advantage is that CNG vehicles place no load on the world's scanty petroleum resources. Methane, CNG's major component, can also be produced from organic substances. This closes the CO<sub>2</sub> cycle and long-term availability is increased even further.

CNG vehicles have proven themselves for years now. Since CNG filling stations are still few and far between, the vehicles are mostly equipped with bi-fuel systems, and the engine can run on either natural gas or gasoline.

CNG has a very high knock resistance (130 ROZ as opposed to between 91 and 100 ROZ for gasoline). This represents further potential for optimization of the CNG engine. This is ideally suited for supercharging, allowing downsizing concepts to be applied with the accompanying improvements in efficiency.

In figure 1 the disposition of Bosch's components of CNG system into car is shown.

#### **CNG engine-management system**

In order to be successful on the market, in addition to their advantages regarding environmental compatibility CNG vehicles must also feature good dynamic response, high driving comfort, and suitability for everyday use. Bosch supports these requirements by developing an engine-management system for CNG vehicles. This comprises the engine-management ECU for the bi-fuel systems (CNG and gasoline), as well as components like pressure regulator module, tank valve, low- and high pressure sensors. During development, the emphasis was on two main points. Firstly the switching between CNG and gasoline operation had to take place without any effects on torque, and secondly, a simple OBD concept was needed. The components were manufactured and tested according to Bosch quality standards, and certified in line with the valid ECE-R110 Standard for CNG vehicles.

In figure 2 the scheme of CNG- system from Bosch is shown.

#### **The bi-fuel NG-Motronic ECU**

This ECU is based on the Motronic version for gasoline injection. It controls the CNG injectors via separate driver stages. The torque-guided control permits the simple integration of the functions which are specific for CNG operation. A number of advantages result from integrating both fuel systems in a bi-fuel ECU. For instance, lower wir-